Methanol Carbonylation Catalyzed by the Anion of the Complex Dicarbonyldiiodorhodium(I). A Density Functional Study of the Catalytic Cycle

Elena A. Ivanova,[†] Philip Gisdakis,[‡] Vladimir A. Nasluzov,*[,†] Anatoly I. Rubailo,[†] and Notker Rösch*[,‡]

Institute of Chemistry and Chemical Technology, Siberian Branch of the Russian Academy of Sciences, Ul. K. Marx 42, 660049 Krasnoyarsk, Russian Federation, and Institut für Physikalische und Theoretische Chemie, Technische Universität München, 85747 Garching, Germany

Received September 1, 2000

The potential energy profile of the full catalytic cycle of methanol carbonylation catalyzed by $[Rh(CO)_2I_2]^-$ complex was explored computationally using a gradient-corrected density functional method. The equilibrium structures of all isomers of the intermediates involved in the catalytic process have been calculated. The transition states of CH_3I oxidative addition, the CO migratory insertion, and the CH_3COI reductive elimination were also located. The rate-determining step of the reaction, CH_3I oxidative addition, was found to proceed via a back-side S_N2 mechanism. The activation barrier of CO migratory insertion is calculated lower than that of CH_3I reductive elimination; this finding confirms the hypothesis that the unstable nature of the complex $[RhCH_3(CO)_2I_3]^-$ is mainly due to its fast decomposition into the acyl species. The trans conformers of the six-coordinated intermediates $[RhCH_3(CO)_2I_3]^-$ and $[Rh(CH_3CO)(CO)_2I_3]^-$ are more stable than their cis conformers. The activation barriers of CO migratory insertion into the Rh−CH_3 bond of $[RhCH_3(CO)_2I_3]^-$ and of CH_3COI reductive elimination from $[Rh(CH_3CO)(CO)_2I_3]^-$ are higher for the trans isomers than those of the corresponding cis isomers. Therefore, the lowest-energy path is determined by the corresponding cis dicarbonyl species which have to be accessed by a ligand rearrangement. Solvent effects of the intermediates were calculated to increase from 6-fold to 5-fold to 4-fold coordinated complexes. While the solvent effects on the transition states are in general similar to those of the six-coordinated complexes, they affect oxidative addition and the reductive elimination steps in a crucial way.

1. Introduction

The carbonylation of methanol to acetic acid catalyzed by rhodium diiodide represents one of the industrially most important processes in homogeneous transition metal catalysis.[1] The catalytic cycle of this classic example of a homogeneous catalytic reaction consists of six steps (Figure 1).[2] The cycle includes several of the main reaction types known in organometallic catalysis[3] such as oxidative addition, ligand migration, CO insertion, and reductive elimination. Such types of elementary steps have separately been examined in a number of theoretical works, e.g., see refs 4−7. Systematic studies including a detailed inspection of full catalytic cycles have been undertaken much less often.[8−10] The catalytic cycle of methanol carbonylation was proposed[2] based on selected data on structures of reactants and intermediates as identified by X-ray crystallography[11]

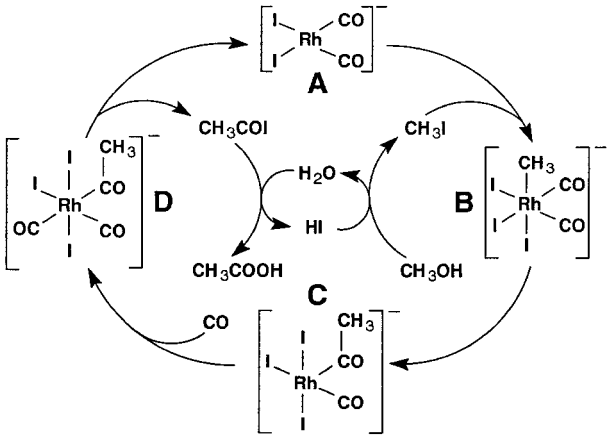

Figure 1. Catalytic cycle of methanol carbonylation to acetic acid. Adapted from ref 20.

[†] Siberian Branch of the Russian Academy of Sciences.
[‡] Technische Universität München.

(1) Herrmann, W. A.; Cornils, B. *Applied Homogeneous Catalysis with Organometallic Compounds*; VCH: Weinheim, 1999.
(2) Forster, D. *J. Am. Chem. Soc.* **1976**, *98*, 846.
(3) Gates, B. C. *Catalytic Chemistry*; Wiley: New York 1992.
(4) Koga, N.; Morokuma, K. *J. Am. Chem. Soc.* **1993**, *115*, 6883.
(5) Sakaki, S.; Ujino, Y.; Sugimoto, M. *Bull. Chem. Soc. Jpn.* **1996**, *69*, 3047.
(6) Sakaki, S.; Ieki, M. *J. Am. Chem. Soc.* **1993**, *115*, 2373.
(7) Albert, K.; Gisdakis, P.; Rösch, N. *Organometallics* **1998**, *17*, 1608.
(8) Matsubara, T.; Koga, N.; Ding, Y.; Musaev, D. G.; Morokuma, K. *Organometallics* **1997**, *16*, 1065.
(9) Dedieu, A. *Inorg. Chem.* **1980**, *19*, 375.
(10) Margl, P.; Ziegler, T.; Blöchl, P. E. *J. Am. Chem. Soc.* **1996**, *118*, 5412.
(11) Forster, D. *Adv. Organomet. Chem.* **1979**, *17*, 255.

10.1021/om000761a CCC: $20.00
Publication on Web 02/15/2001

and infrared and NMR spectroscopies.[12] The anion $[Rh(CO)_2I_2]^-$ (**A**) was found to be the initial catalytically active species.[2] Its interaction with the substrate CH_3I results in the formation of the six-coordinated complex $[RhCH_3(CO)_2I_3]^-$ (**B**)[12] (Figure 1), which is kinetically unstable; it transforms into the isomeric five-coordinated acetyl complex $[Rh(CH_3CO)(CO)I_3]^-$ (**C**) as a result of the migration of the methyl group to the CO ligand.[13] The rhodium acetyl complex **C** is the only stable intermediate of the catalytic cycle;[11] it was isolated, and its structure was determined by X-ray crystallography.[14,15] The rhodium acetyl anion **C** was found to form dimers through a very weak Rh−I−Rh bridge (with r(Rh−I) = 3.0 Å, compared to 2.7 Å commonly found for Rh−I coordination bonds[14]). Complex **C** reacts rapidly with CO to form the six-coordinated dicarbonyl complex **D** with terminal CO (Figure 1);[15] this species has been characterized by IR and NMR spectroscopy as a trans isomer.[16] An isomerization to a cis isomer was proposed to facilitate the subsequent elimination of CH_3COI.[16] The cis isomer decomposes at room temperature to yield acetyliodide CH_3COI and $[Rh(CO)_2I_2]^-$; the latter species starts the next catalytic cycle. Finally, acetyl iodide hydrolysis leads to the formation of the target product, acetic acid.

Kinetic investigations have shown that the rate of methanol carbonylation depends on the concentrations of both the rhodium complex and methyliodide.[17] From this finding, it was deduced[2] that oxidative addition of CH_3I to $[Rh(CO)_2I_2]^-$ is the rate-determining step of the catalytic cycle. The mechanism of this step has already been theoretically investigated using Hartree−Fock (HF) theory.[18] However, a computational investigation with a more reliable quantum chemical approach that in particular accounts for correlation effects during the geometry optimization and solvent effects is still lacking. The second step of the reaction cycle (Figure 1), CO migratory insertion **B** → **C**, has recently been explored with a density functional method.[19] The third step, CO uptake, and the final step, CH_3COI reductive elimination, have not yet been theoretically investigated to our knowledge. A systematic and complete analysis of the whole catalytic cycle in the framework of a uniform theoretical approach has never been undertaken.

In this work we present a density functional investigation of the cycle of the methanol carbonylation reaction $CH_3OH + CO \rightarrow CH_3COOH$ catalyzed by the rhodium complex $[Rh(CO)_2I_2]^-$. Actually, only the outer cycle (see Figure 1) which involves the organometallic compounds is of interest in the present work; the purely organic steps, namely, the formation of CH_3I from methanol and the hydrolysis of CH_3COI to acetic acid, will not be considered in the following.

We will check the hypothesis[12,13] that the unstable intermediate **B** preferentially decays to **C** via migratory insertion (with a low activation barrier) rather than decomposing back to CH_3I and **A** via reductive elimination. Special attention will be paid to the acetyliodide reductive elimination step **D** → **A**, which becomes overall rate-determining at temperatures below 30 °C, whereas CH_3I oxidative addition was found to be rate-limiting at reaction conditions.[20] We will also reinvestigate the mechanism of the CH_3I oxidative addition step **A** → **B** with a density functional method. In a previous study[18] two transition states (TS) were located at the restricted HF level. The direct methyl attack at the metal center, corresponding to the classic S_N2 mechanism,[21,22] was calculated[18] to have a lower activation barrier than the alternative C−I side-on approach. However, the TS structures of the former study[18] were optimized at the HF level only, and reinvestigation at a level of theory that involves electron correlation seems warranted.

Since the reaction rate shows a significant dependence on the reaction medium,[23] solvent effects need to be computationally investigated because for charged species as in this catalytic process they are expected to strongly affect the activation barrier of the overall process. In short, the goals of this paper are

- to theoretically quantify structural parameters of reactants, intermediates, and products participating in the rhodium-catalyzed carbonylation of methanol,
- to locate transition states for each step of the catalytic cycle,
- to construct an overall energy profile of the reaction cycle, and
- to estimate solvent effects on the energies of intermediates and transition states.

2. Computational Details

Density functional calculations were performed with the program suite Gaussian98.[24] The geometries of all of intermediates as well as the corresponding transition states were optimized. D_{2h} and C_{2v} symmetry constraints were imposed for the trans and cis isomers of the four-coordinated complex **A**, respectively. All other species **B**, **C**, and **D** were optimized with C_s symmetry constraints. No symmetry restrictions were applied during transition state searches. Transition states were located by employing a reaction coordinate method followed by a transition state search based on the Berny algorithm as implemented in Gaussian98.[24] The Hessians of all transition states were checked to have exactly one negative

(12) Haynes, A.; Mann, B. E.; Morris, G. E. Maitlis, P. M. *J. Am. Chem. Soc.* **1993**, *115*, 4093.
(13) Bassetti, M.; Monti, D.; Haynes, A.; Pearson, J. M.; Stanbridge, I. A.; Maitlis, P. M. *Gaz. Chim. Ital.* **1992**, *122*, 391.
(14) Adamson, G. W.; Daly, J. J.; Forster, D. *J. Organomet. Chem.* **1974**, *71*, C17.
(15) Adams, H.; Bailey, N. A.; Mann, B. E.; Manuel, C. P.; Spencer, C. M.; Kent, A. G. *J. Chem. Soc., Dalton Trans.* **1988**, 489.
(16) Howe, L. A.; Bunel, E. E. *Polyhedron* **1995**, *14*, 167.
(17) Roth, J. F.; Craddock, J. H.; Hershman, A.; Paulik, F. E. *Chem. Technol.* **1971**, 600.
(18) Griffin, T. R.; Cook, D. B.; Haynes, A.; Pearson, J. M.; Monti, D.; Morris, G. E. *J. Am. Chem. Soc.* **1996**, *118*, 3029.
(19) Cheong, M.; Schmid, R.; Ziegler, T. *Organometallics* **2000**, *19*, 1973.
(20) Maitlis, P. M.; Haynes, A.; Howard, M. J. *J. Chem. Soc., Dalton Trans.* **1996**, *11*, 2187.
(21) Chatt, J.; Shaw, B. L. *J. Chem. Soc.* **1959**, 705.
(22) Chock, P. B.; Halpern, J. *J. Am. Chem. Soc.* **1966**, *88*, 3511.
(23) Hickey, C. E.; Maitlis, P. M. *J. Chem. Soc., Chem. Commun.* **1984**, 1609.
(24) Frisch, M. J.; Trucks, G. W.; Schlegel, H. B.; Scuseria, G. E.; Robb, M. A.; Cheeseman, J. R.; Zakrzewski,V. G.; Montgomery, J. A.; Stratmann, Jr.; Burant, R. E., J. C.; Dapprich, S.; Millam, J. M.; Daniels, A. D.; Kudin, K. N.; Strain, M. C.; Farkas, O.; Tomasi, J.; Barone, V.; Cossi, M.; Cammi, R.; Mennucci, B.; Pomelli, C.; Adamo, C.; Clifford, S.; Ochterski, J.; Petersson, G. A.; Ayala, P. Y.; Cui, Q.; Morokuma, K.; Malick, D. K.; Rabuck, A. D.; Raghavachari, K.; Foresman, J. B.; Cioslowski, J.; Ortiz, J. V.; Stefanov, B. B.; Liu, G.; Liashenko, A.; Piskorz, P.; Komaromi, I.; Gomperts, R.; Martin, R. L.; Fox, D. J.; Keith, T.; Al-Laham, M. A.; Peng, C. Y.; Nanayakkara, A.; Gonzalez, C.; Challacombe, M.; Gill, P. M. W.; Johnson, B.; W. Chen, W.; Wong, M. W.; Andres, J. L.; Gonzalez, C.; Head-Gordon, M.; Replogle, E. S.; Pople, J. A. *Gaussian 98*, Revision A.3; Gaussian, Inc.: Pittsburgh, PA, 1998.

Table 1. Calculated Bond Distances (in Å) and Bond Angles (in deg) of Intermediates[a] and Their Isomers Involved in the Methanol Carbonylation Cycle as Well as Energies ΔE (in kJ/mol) Relative to A1

	A1	A2	B1	B2	B3	C	D1	D2	D3
Rh−C1	1.853	1.912	1.885	1.925	1.868	1.866	1.901	1.927	1.869
Rh−C2			2.151	2.150	2.134	2.012	2.119	2.070	2.103
Rh−C3					2.010				2.076
Rh−I1	2.775	2.749	2.802	2.791	2.805	2.761	2.798	2.801	2.808
Rh−I2			2.930	2.879	2.823	2.795	3.003	2.939	2.856
C2−C4						1.530	1.518	1.533	1.527
C1−O1	1.164	1.158	1.155	1.151	1.156	1.157	1.153	1.152	1.154
C2−O2						1.202	1.208	1.209	1.212
C3−O3					1.150				1.149
I1−Rh−I1	95.8	180.0	96.7	174.4	174.4	172.7	96.4	168.0	171.3
I1−Rh−C1	179.9	90.0	178.4	90.4	87.2	87.5	82.0	92.0	88.0
Rh−C1−O1	177.5	180.0	176.6	179.7	179.0	176.0	176.6	177.7	177.3
C2−Rh−C1			92.9	91.8	85.6	90.1	91.7	92.2	87.0
C2−Rh−I1			87.0	85.6	89.4	92.7	95.0	84.3	86.0
C2−Rh−I2			175.1	178.6	90.8	108.8	167.1	178.6	99.8
C2−Rh−C3					173.2				177.0
ΔE[b]	0.0	32.6	−19.0	−28.3	−17.5	−64.4	−117.8	−126.4	−100.3
ΔE[c]	0.0	37.5	−25.4	−31.0	−22.7	−62.8	−122.2	−127.5	−102.1

[a] For structures and notations, see Figure 2. [b] Standard basis set. [c] Extended basis set (decontracted at the Rh center and supplemented by an Rh f-exponent; see text).

eigenvalue. For the transition state **TS(A1-B1)(n)$_{back}$** of the neutral model $[Rh(CO)_2I_2]^-/CH_3I/NH_4^+$ (see section 3.2.1) an exception had to be made. In that case, due to numerical instabilities of the algorithm used, the structure was not completely optimized. Besides one imaginary frequency of 118i cm^{-1} which describes the stretching of the bond of interest (Rh−C), the structure located exhibits three further small imaginary frequencies (29i, 22i, and 6i cm^{-1}) associated with such soft modes as the rotations of the NH_4 group.

We employed the gradient-corrected exchange functional proposed by Becke[25] in combination with the gradient-corrected correlation functional of Perdew[26] (BP86); all Kohn−Sham calculations were performed in spin-restricted fashion. For the heavy elements Rh and I, Hay−Wadt effective core potentials[27,28] (in combination with standard double-ζ basis sets, LANL2DZ) were used to replace the core electrons up to 3d. The first-row elements were described by 6-311G(d,p) basis sets. To obtain more accurate energy estimates, an extended basis set was applied in single-point fashion at the previously optimized geometries. This extended basis set was decontracted[29] at the Rh center and augmented by one Rh f-type polarization exponent.[30] The relative energies of the various reaction intermediates calculated by both basis sets are very similar, with maximum differences of 6 kJ/mol (see Table 1). The more flexible basis set resulted in changes of the activation energies by at most 7 kJ/mol (see Table 2). In the following we will only discuss the energetics calculated with the extended basis set.

Changes of the Gibbs free reaction energy $\Delta G(X\rightarrow Y)$ in the gas phase were calculated by taking zero-point energies, thermal motion, and entropy contributions at standard conditions (temperature 298.15 K, pressure 1 atm) into account. The main difference between ΔE and ΔG values is caused by the entropy contribution $T\Delta S$ of about 50 kJ/mol for reactions where the number of independent species changes by 1; other terms are about 1 order of magnitude smaller.

Solvent effects were estimated by employing the integral equation formalism of the polarizable continuum model.[31] Environment effects were estimated for dichloromethane CH_2Cl_2 (dielectric constant $\epsilon = 8.9$ measured at 25 °C), one of the experimentally used solvents.[20] The contributions of the solvent effects were accounted for via the free solvation energy $\Delta G_{solv}(Y)$ at the stationary point Y. $\Delta G_{solv}(Y)$ was estimated as

$$\Delta G_{solv} = \Delta G_{el} + \Delta G_{cav} + \Delta G_{disp} + \Delta G_{rep} \quad (1)$$

Here, ΔG_{el} is the electrostatic contribution, ΔG_{cav} is the energy required to form a suitable cavity in the solvent, and ΔG_{disp} and ΔG_{rep} are the dispersion and repulsion contributions, respectively, due to the nonbonded interactions. The final free reaction energy in solution $\Delta G_{final}(X\rightarrow Y)$ was calculated as

$$\Delta G_{final}(X\rightarrow Y) = \Delta G(X\rightarrow Y) + \Delta G_{solv}(Y) - \Delta G_{solv}(X) \quad (2)$$

where $\Delta G(X\rightarrow Y)$ is the free reaction energy in the gas phase.

3. Results and Discussion

In the following, we will first present the structure and relative energies of all intermediates as well as their possible isomers (Tables 1 and 3, Figures 2 and 3). Subsequently, we will describe the mechanism of each elementary step of the catalytic cycle and the structure of the corresponding transition state (Table 2, Figures 4 and 5). Then we will discuss solvent effects, and finally we will construct a free energy profile of the entire catalytic cycle (Tables 4 and 5, Figures 6 and 7).

3.1. Intermediates. As noted in the Introduction, except for the acyl−rhodium complex **C**, no structural data on the intermediates **A**, **B**, and **D** of the methanol carbonylation cycle are available from experiment because of the instability of these species; complex **C** was isolated as a dimer and structurally characterized.[15] For species **A**, **B**, and **D**, structures have been proposed based on spectroscopic data.[12] All intermediates are likely to exist in an equilibrium of several isomers. In this section we will discuss the gas-phase-optimized geometries of the intermediates and relative energies of their isomers.

(25) Becke, A. D. *Phys. Rev. A* **1988**, *38*, 3098.
(26) Perdew, J. P. *Phys. Rev. B* **1986**, *33*, 8822.
(27) Wadt, W. R.; Hay, P. J. *J. Chem Phys.* **1985**, *8*, 284.
(28) Wadt, W. R.; Hay, P. J. *J. Chem Phys.* **1985**, *82*, 299.
(29) Frenking, G.; Antes, I.; Böhme, M.; Dapprich, S.; Ehlers, A. W.; Jonas, V.; Neuhaus, A.; Otto, M.; Stegmann, R.; Veldkamp, A.; Vyboishchikov S. F. *Reviews in Computational Chemistry*; Lipkowitz, K. B., Boyd D. B., Eds.; VCH: New York, 1996; Vol. 8, p 63.
(30) Ehlers, A. W.; Böhme, M.; Dapprich, S.; Gobbi, A.; Höllwarth, A. H.; Jonas, V.; Köhler, K. F.; Stegmann, R.; Veldkamp, A.; Frenking, G, *Chem. Phys. Lett.* **1993**, *208*, 111.
(31) Amovili, C.; Barone, V.; Cammi, R.; Cances, E.; Cossi, M.; Mennucci, B.; Pomelli, C. S.; Tomasi, J. *Adv. Quantum. Chem.* **1999**, *32*, 227.

Table 2. Optimized Distances (in Å) and Angles (in deg) of Transition States TS of Various Steps of the Methanol Carbonylation Cycle: CH_3I Oxidative Addition, CO Migratory Insertion, and CH_3COI Reductive Elimination[e]

TS	A1-B1$_{back}$	A1-B3(n)$_{front}$	A1-B1$_{front}$	A1-B3$_{front}$	B1-C	B2-C	B3-C	D1-A1	D3-A2	D3-A1
Rh−C1	2.960	2.858	2.766	2.753	2.369	2.378	2.319			-
Rh−C2	1.871	1.918	1.870	1.904	1.876	1.912	1.877	2.564	2.783	2.863
Rh−C3	1.871	1.857	1.866	1.859	1.887	1.975	1.878	1.858	1.912	1.855
Rh−C4								1.879	1.932	1.901
Rh−I1	5.163	2.945	2.926	2.912	2.905	2.781	2.790	2.789	2.755	2.809
Rh−I2	2.753	2.845	2.803	2.807	2.795	2.781	2.790	3.344	3.972	3.015
Rh−I3	2.753	2.797	2.950	2.894	2.769	2.763	2.866	2.842	2.755	2.866
C1−C2					1.937	1.853	1.968	1.514	1.508	1.501
C1−I1[a]	2.543	2.712	2.629	2.675						-
C2−I2[b]								2.491	2.446	2.517
C2−O2	1.157	1.156	1.163	1.160	1.172	1.175	1.171	1.198	1.189	1.187
C3−O3	1.158	1.155	1.160	1.161	1.157	1.153	1.155	1.163	1.156	1.161
C4−O4								1.157	1.153	1.161
I1−C1−Rh	139.4	63.8	65.6	64.9						-
C1−Rh−I1	-	55.7	54.9	56.3	101.3	88.7	90.5			-
C2−Rh−I3	83.5	121.6	114.1	119.8	105.7	100.7	154.9	134.1	96.6	74.7
C1−Rh−C3	98.5	95.9	96.7	95.9	98.6	116.5	170.3			-
C1−Rh−I3	84.8	76.1	147.6	78.1	158.4	150.4	100.2			-
Rh−C2−O2	177.5	173.0	174.8	174.6	164.3	163.1	167.6			-
C2−Rh−I2	177.3	82.7	82.2	82.5	86.6	90.8	88.1	47.6	37.5	50.6
C3−Rh−I3	176.6	82.7	80.6	81.6	85.1	93.0	89.5	142.7	89.3	84.4
C4−Rh−I3								79.8	88.7	126.1
C4−Rh−C3								96.7	169.9	95.0
ΔE[c]	147.4	158.4	136.4	132.4	72.9	78.7	38.8	67.9	56.5	77.2
ΔE[d]	146.0	157.6	136.3	132.4	75.5	81.0	40.2	72.7	63.8	79.6

[a] The C−I bond length of free CH_3I is calculated as 2.193 Å. [b] The C−I bond length of the free molecule CH_3COI is calculated as 2.300 Å. [c] Standard basis set. [d] Extended basis set (decontracted at the Rh center and supplemented by an Rh f-exponent). [e] Also given are the corresponding activation energies ΔE (in kJ/mol).

Table 3. Comparison of Calculated and Experimental Bond Lengths (in Å) of the Rhodium−Acyl Complex C and Its Dimer CC (see Figures 2 and 3)

bond distance	calc(**C**)	calc(**CC**)	exptl[a]	exptl[b]
Rh−C1	1.866	1.871	1.860	1.834
Rh−C2	2.012	2.030	2.062	2.132
Rh−I1	2.761	2.785	2.652	2.666
Rh−I2	2.795	2.820	2.699	2.857
C2−C4	1.530	1.526	1.308	1.356
C1−O1	1.157	1.154	1.061	1.116
C2−O2	1.202	1.210	1.257	1.141
Rh−I3[c]		2.784	2.679	
Rh−I3[d]		3.271	3.001	

[a] Dimer **CC** (ref 14). [b] Complex **C** with pyridine as an extra ligand (ref 15). [c] Short distance between Rh and bridging I3 group. [d] Long distance between Rh and bridging I3 group.

3.1.1. Initial Four-Coordinated Complexes A. The interaction of CH_3I with the planar complex **A** starts the catalytic cycle. This initial complex **A** has cis and trans isomers, denoted as **A1** and **A2**; see Figure 2. Their optimized geometry parameters and relative energies are presented in Table 1. As one can see, in **A2**, where the two iodide ligands are in trans position to each other, Rh−I bonds are shorter (2.749 Å) than in **A1** (2.775 Å), where each iodine is trans to a carbonyl ligand. Concomitantly, the Rh−C bond in **A2**, trans to the CO ligand, is 0.06 Å longer than the Rh−C bonds of **A1**. These data indicate that carbonyl ligands weaken bonds in trans position more than iodide ligands. The angles between two CO ligands and those between the two iodide ligands in the cis complex are slightly larger than 90°; this can be ascribed to the electronic repulsion between π electrons of the oxygen centers and the steric repulsion between the iodide ligands. (Note that the van der Waals radius of I is 1.98 Å,[32] whereas the distance I−I in **A1** is 4.1 Å.)

Isomer **A1** with cis carbonyl groups is more stable than the corresponding trans isomer **A2** by 38 kJ/mol (34 kJ/mol in a recent DF study[19]). This is in agreement with experiment in which the initial catalytically active complex has been characterized as a cis isomer.[11]

3.1.2. Six-Coordinated Complexes B. The six-coordinated complex **B** is the product of CH_3I oxidative addition to the four-coordinated reactant **A**. The three possible structures **B1**, **B2**, and **B3** of complexes **B**, all of them only slightly distorted from the ideal octahedral coordination, are shown in Figure 2. The iodide ligand I2 of isomer **B1** is bent toward the carbonyl groups; in isomer **B3** the carbonyl ligand C3O3 in trans position of the methyl group is bent toward the iodide centers. As already noted, these structural features may be rationalized in terms of steric interaction among the three iodide ligands and electronic repulsion between the CO groups, respectively. Comparing the bond distances of the complexes **B** (Table 1), one observes an increasing bond elongation in trans position to the ligand in the series I < CO < CH_3. The Rh−I bond distance increases in that order when I is in trans position to I (2.79−2.80 Å, I1 in **B2** and **B3**), CO (2.80−2.82 Å, I1 in **B1** and I2 in **B3**), and the CH_3 group (2.88−2.93 Å, I2 in **B1** and **B2**). The Rh−carbonyl distance also elongates in the same order, from 1.87−1.89 Å (C1 in **B1** and **B3**) to 1.92 Å (C1 in **B2**) and 2.01 Å (C3 in **B3**), with CO in trans position to iodine, carbonyl, and methyl, respectively. The Rh−methyl bond length Rh−C2 trans to the carbonyl (see isomer **B3**, 2.13 Å) is slightly shorter than that in the two other complexes **B1** and **B2**, where the methyl group is in trans position to an iodide ligand (2.15 Å).

All isomers of type **B** exhibit relatively similar energies (Table 1). **B2** is calculated to be the most stable

(32) Bondi, A. *J. Phys. Chem.* **1964**, *68*, 441.

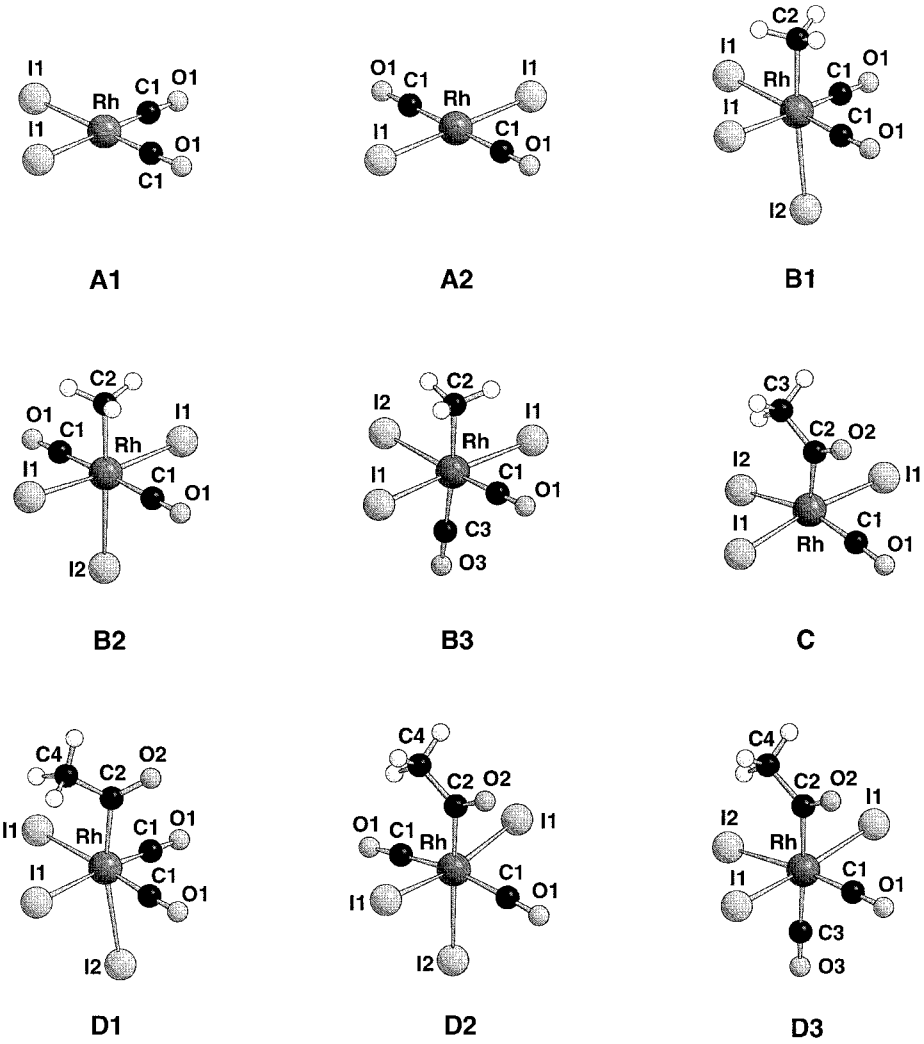

Figure 2. Structures of the most important intermediates of the methanol carbonylation cycle.

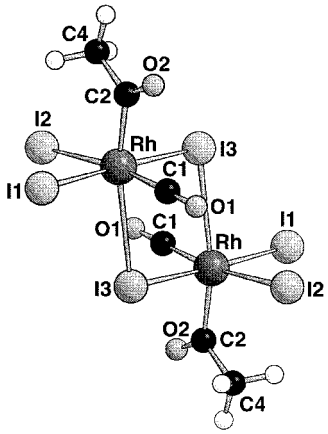

Figure 3. Structure of the dimer **CC** of complex **C**.

isomer; its energy is about 6 and 8 kJ/mol lower than that of **B1** and **B3**, respectively. The energy difference of 2 kJ/mol for the latter is not significant, and the two isomers **B1** and **B3** may be considered isoenergetic. It is worth noting that a small energy preference of isomer **B1** over species **B2** and **B3** of 1 and 4 kJ/mol, respectively, has also been reported in a previous DF study.[19] From NMR and IR data, the intermediate formed after CH_3I oxidative addition to the square-planar complex **A** was deduced to be isomer **B1**.[12] In NMR, only one doublet was observed in the rhodium carbonyl region, indicative of equivalent carbonyl ligands, as in **B1** and **B2**. In the IR spectrum, two carbonyl bands were found to have similar intensities, as expected for the cis dicarbonyl species **B1**. However, the spectroscopic data reported in ref 12 do not provide direct information on the number of iodide ligands in complex **B**. Alternative structures of the observed intermediate are the neutral five-coordinated species $[Rh(CO)_2I_2CH_3]^-$ or, more likely in solution, a neutral solvent complex $[Rh(CO)_2I_2CH_3$-(solvent)].

Yet another rationalization of the observation of complex **B1** instead of the more stable isomer **B2** can be proposed. Complex **B2** forms after addition of CH_3I to **A2**, but the lower stability of the latter complex compared to **A1** prevents the reaction **A2** → **B2** from proceeding. Thus, initial formation of **B1** by addition of CH_3I to **A1** is favored. In the next step, the rearrangement **B2** → **C** by CO migration exhibits a higher barrier than the analogous processes **B1** → **C** and **B3** → **C** (see section 3.2.2). Thus, in the overall dynamics, **B2** isomerizes to **B1** or **B3** to permit a reaction path with a lower barrier for CO migration. Thus, complex **B2** is not observed because of fast conversion to other isomers and small concentration. Therefore, to arrive at a description consistent with available experimental information, it is necessary to estimate activation energy barriers for the various elementary steps (see below).

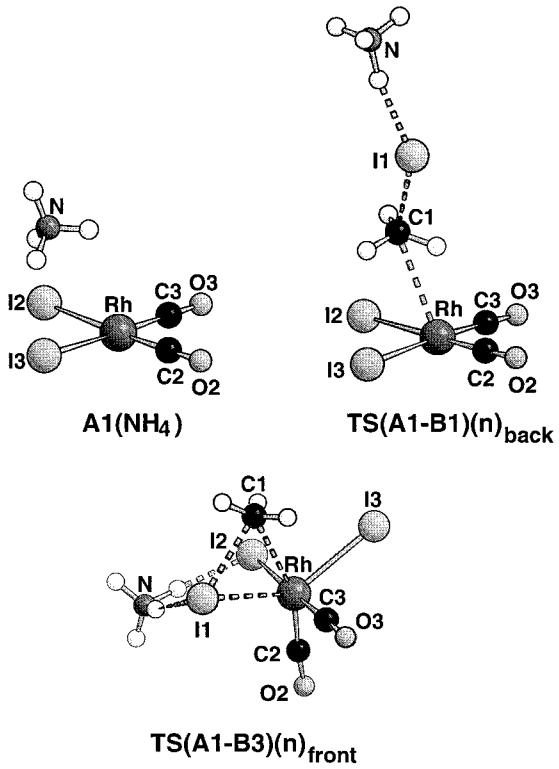

Figure 4. Structures of the coordinated with cation NH_4^+, neutral species **A1(NH$_4$)**, and transition states, **TS(A1-B1)(n)$_{back}$** and **TS(A1-B3)(n)$_{front}$**, of CH_3I oxidative addition **A** → **B** via back-side and front-side mechanisms, respectively.

3.1.3. Five-Coordinated Complex C. The five-coordinated complex **C** is the product of CO insertion into the Rh−CH_3 bond of **B**-type complexes (Figure 1). As expected for the d^6 system,[33] **C** exhibits a square-pyramidal structure. There are four possible isomers of type **C** with I, CO, or acyl groups in the axial position. In our calculations all such starting structures converged to the structure with the acyl group in axial position (see Figure 2). This apical preference of CH_3-CO can be rationalized in terms of the stronger trans-directing influence of this ligand than that of iodine and carbonyl.[33] In other words, a Rh−ligand bond in trans position to the CH_3CO group would be elongated more than bonds trans to CO or I groups, and such a conformer would be the least stable one. Therefore, the structure with a vacant position trans to the acyl ligand is preferred.

The Rh−I1 bonds of **C** (with two iodine ligands in trans position to each other) are 0.03−0.04 Å shorter than the corresponding bonds of complexes **B** (I1 in **B2**, **B3**). The Rh−I2 bond of **C** with I trans to a CO ligand is comparable to the corresponding bond of **B1** (Rh−I1), but again 0.03 Å shorter than that in **B3**. The Rh−C1 bond length of the carbonyl ligand of **C** was calculated essentially the same as in the other structures with CO in trans position to an iodide ligand (**A1**, **B1**, **B3**). Hence, we can conclude that bond distances in the equatorial plane of complex **C** remain essentially unchanged compared to species of type **B**.

Complex **C** provides an opportunity to compare calculated distances with experimental data since it is the only one whose analogues have been structurally characterized.[14,15] Complex **C** has been isolated as a dimer with two bridging iodine moieties[14] and as a six-coordinated complex with pyridine as an extra ligand.[15] Under reaction conditions species **C** is likely coordinated in addition by a solvent molecule, e.g., by methanol.[15] In Table 3 we compare bond distances of complex **C** and related systems. To render the comparison more direct, we have also optimized the structure of the dimer **CC** of complex **C** (see Table 3 and Figure 3). The calculated Rh−$COCH_3$ (Rh−C2) bond length, 2.012 (**C**) and 2.030 (**CC**) Å, is in reasonable agreement with the experimental value of Adamson et al.,14 2.062 Å. An Rh−acyl bond distance similar to our results (2.012 Å) was obtained in a BP calculation of the complex $RhH(CH_3CO)(PH_3)_2Cl$.[10] The other experimental value, 2.132 Å, reported by Adams et al.,[15] is significantly longer than common Rh−$COCH_3$ bond distances of such complexes, which are about 2.00 Å.[15] The calculated Rh−CO bond length, 1.866 (**C**) and 1.871 (**CC**) Å, correlates with the experiment, 1.860 Å,[14] even better than the Rh−C(acyl) distance. Calculated Rh−iodide ligand bond lengths, in general, are overestimated by about 0.1 Å as compared to experiment. The Rh−I bridge (long Rh−I3 bond in Table 3) of the binuclear rhodium complex **CC** is calculated to be 0.27 Å longer than the experimental value (Table 3). The observed overestimation of the Rh−I bond lengths can in part be attributed to a known feature of gradient-corrected DF functionals, which often tend to overestimate bond lengths.[34] However, it should be noted that similar discrepancies for calculated and observed rhodium−iodine bond lengths have previously been obtained in HF calculations with the LANL2DZ basis.[35] A rather long experimental Rh−I distance, 2.857 Å,[15] was determined for iodine in trans position to the acyl group, which is known to exert a strong trans influence; such a ligand coordination is absent in the calculated structure of complex **C** (Figure 2).

There are more differences between our calculated structures and available experimental data.[14,15] We first mention the C−C bond length of the acyl group. The calculated distances of 1.530 Å (**C**) and 1.526 (**CC**) Å are about 0.2 Å longer than the experimental values, 1.308 and 1.356 Å.[14,15] However, the latter distances are rather small compared to typical lengths of C−C single bonds; for example, that of CH_3CHO is measured to be 1.50 Å.[36] In a previous BP calculation[10] on a Rh complex the C−C distance of an acyl ligand was calculated to be 1.520 Å, in good agreement with the present results. The C−O bond distance of the carbonyl group reported in ref 14, 1.061 Å, and ref 15, 1.116 Å, is also unusually short. The calculated values, 1.157 (**C**) and 1.154 (**CC**) Å, agree well with commonly observed experimental[3] and BP calculated[10] values for carbonyl groups (1.13−1.15 Å). Discrepancies from experimental C−O distances of the acyl group, 1.257[14] and 1.141 Å,[15] also have to be noted. However, our calculated acyl C−O distances, 1.202 (**C**) and 1.210 (**CC**) Å, are in good agree-

(33) Albright, T. A.; Burdett, J. K.; Whangbo, M. H. *Orbital Interaction in Chemistry*; Wiley: NewYork, 1984.

(34) Johnson, B. G.; Gill, P. M. W.; Pople, J. A. *J. Chem. Phys.* **1993**, *98*, 5612.

(35) Koga, N.; Morokuma, K. *J. Phys. Chem.* **1990**, *94*, 5454.

(36) *CRC Handbook of Chemistry and Physics*, 59th ed.; CRC Press: Boca Raton, FL, 1978−1979.

(37) Daly, J. J.; Sanz, F.; Forster, D. *J. Am. Chem. Soc.* **1975**, *97*, 2551.

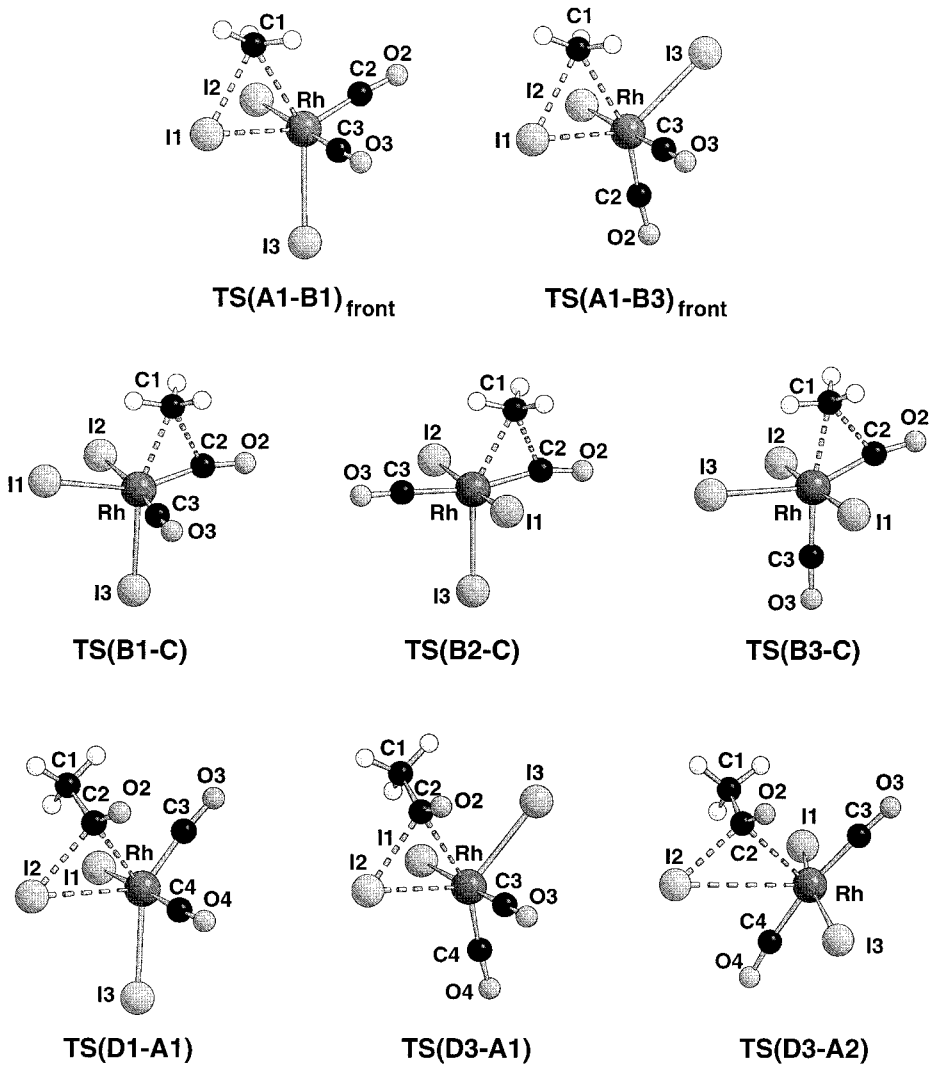

Figure 5. Structures of the transition states for various elementary steps of the methanol carbonylation cycle: CH_3I oxidative addition (via front-side mechanism), CO migratory insertion, and CH_3COI reductive elimination.

ment with the BP value reported[10] for the rhodium acyl complex $RhH(CH_3CO)(PH_3)_2Cl$, 1.21 Å. The calculated parameters of the acyl group and the carbonyl ligand for the systems under discussion may be considered more reliable than the corresponding experimental values[14,15] because DF methods are known to accurately reproduce structural parameters and discrepancies as those found here are unusual.

The dimerization of complex **C** is calculated to be very endothermic, by 186 kJ/mol (see Table 4), since the association of two negatively charged particles is very unfavorable in the gas phase. Hence, the dimerized structure of complex **C** found in the solid state is strongly stabilized by the Coulomb field of the crystal environment and thus may differ from the gas-phase structure. The stability of dimer **CC** in solution will be discussed in section 3.3.

3.1.4. Six-Coordinated Complexes D. The six-coordinated acetyl complex **D** is the product of CO addition to the five-coordinated complex **C**. It is also the precursor of the last reaction step, acetyliodide elimination (Figure 1). The isomers of complex **D** are analogous to those of complexes **B**, with the CH_3 group replaced by an acetyl group. Three isomers of **D**-type complexes have been calculated (see Table 1 and Figure 2). The Rh−ligand bond distances in trans position to the acyl group (Rh−I2 in **D1** and **D2**, Rh−C3O3 in **D3**) are elongated by 0.05−0.07 Å compared to the corresponding **B**-type complexes, where these ligands are in trans position to methyl group. Thus, the trans-directing effect of the acyl ligand is comparable to that of the methyl ligand. The Rh−acyl bond distance Rh−C2 varies slightly among the three isomers. Because of CO or I ligands trans to the acyl group, the Rh−acyl bond of the complexes **D** is 0.06−0.11 Å longer than in complex **C**, where the position trans to the acyl group is vacant. It is interesting to note that the Rh−acyl bond Rh−C2 is shorter by 0.03−0.08 Å than the corresponding Rh−methyl bond of complexes **B**, while the corresponding C−I bond length of CH_3COI (2.30 Å) is calculated longer than the C−I bond of CH_3I (2.19 Å). Such a shortening of the Rh−C bond due to a change in hybridization at the carbon center ($sp^3 \rightarrow sp^2$) has already been observed earlier.[38]

Just as for the series of complexes **B**, species **D2** with CO ligands in trans position to each other is calculated as the most stable of the **D**-type isomers (Table 1). Isomers **D1** and **D3** lie 5 and 25 kJ/mol, respectively,

(38) Siegbahn, P. E. M. *J. Phys. Chem.* **1995**, *99*, 12723.

Table 4. Free Energies ΔG_{solv}(Y) of Solvation of Selected Stationary Points Y, Reaction Energies ΔE(X→Y), and Free Reaction Energies ΔG(X→Y) in the Gas Phase and Estimates of the Free Reaction Energies ΔG_{Final}(X→Y) in Dichloromethane[g]

X	Y	ΔE(X→Y)	ΔG(X→Y)	ΔG_{solv}(Y)	ΔG_{final}(X→Y)
	A1(NH$_4$)			−31.1	
A1(NH$_4$)[a]	**TS(A1-B1)(n)$_{back}$**	146.0	188.7	−94.4	134.8
A1(NH$_4$)[a]	**TS(A1-B3)(n)$_{front}$**	157.6	195.3	−42.0	193.8
A1[a]	**TS(A1-B1)$_{front}$**	136.3	177.2	−129.3	195.3
A1[a]	**TS(A1-B3)$_{front}$**	132.4	174.4	−125.1	196.9
A1	**A2**	37.5	39.4	−138.0	39.3
A1[a]	**B1**	−25.4	23.6	−129.2	41.9
A2[a]	**B2**	−68.4	−18.8	−127.6	1.0
A1[a]	**B3**	−22.7	25.0	−125.9	46.5
A2[a]	**B3**	−60.2	−14.4		7.2
B1	**TS(B1-C)**	75.5	76.5	−131.1	74.5
B2	**TS(B2-C)**	81.0	80.1	−130.5	77.2
B3	**TS(B3-C)**	40.2	43.8	−127.8	42.0
B1	**C**	−37.4	−29.2	−130.8	−30.7
B2	**C**	−31.8	−26.0		−29.1
B3	**C**	−40.1	−30.6		−35.4
C[b]	**CC**	186.4	233.8	−408.7	86.6
C[c]	**D1**	−59.4	−14.9	−124.5	−8.9
C[c]	**D2**	−64.8	−17.5	−124.2	−11.2
C[c]	**D3**	−39.3	6.4	−122.0	14.8
D1	**TS(D1-A1)**	72.7	74.2	−123.7	75.0
D3	**TS(D3-A2)**	63.8	57.9	−96.3	83.7
D3	**TS(D3-A1)**	79.6	77.7	−126.5	73.3
D1	**A1**[d]	48.8	−0.7	−138.0	−27.3
D2	**A2**[d]	91.6	41.3		14.5
D3	**A2**[d]	66.2	17.5		−11.5
D3	**A1**[d]	28.7	−21.9		−50.9
A1[e]	**A1**[d]	−73.4	−21.1		−24.9

[a] Energy of free CH_3I added to that of complexes **A**. [b] Energy of a second unit **C** added to that of complex **C**. [c] Energy of free CO was added to that of complex **C**. [d] Energy of free CH_3COI added to that of complexes **A**. [e] Energy of free CH_3I and CO added to that of **A1**. [f] The free energies of solvation for CH_3I, CO, and CH_3COI are −9.5, 0.3, and −13.0 kJ/mol, respectively. [g] All quantities (in kJ/mol) are calculated with the extended basis set.

Table 5. Calculated (in kJ/mol, standard basis set) Enthalpy at 0 K (ΔH^0) and 298 K (ΔH^{298}) and Gibbs Free Energy (ΔG) for Intermediates and Transition States of Methanol Carbonylation Catalytic Cycle with Respect to A1 + CH_3I

	ΔE	ΔZPE[a]	ΔH^0	ΔE_{therm}[b]	ΔH^{298}	$T\Delta S$	ΔG	$\Delta G - \Delta E$
TS(A1-B1)(n)$_{back}$[c]	147.4	−5.4	142.0	−1.9	140.1	−50.0	190.1	42.7
TS(A1-B3)(n)$_{front}$[c]	158.4	−4.7	153.7	3.2	156.9	−39.2	196.1	37.7
TS(A1-B1)$_{front}$	136.4	−3.6	132.8	1.9	134.7	−42.6	177.3	40.9
TS(A1-B3)$_{front}$	132.4	−4.3	128.1	1.8	129.9	−44.5	174.4	42.0
B1	−19.0	1.9	−17.1	1.7	−15.4	−45.4	30.0	49.0
B2	−28.3	1.5	−26.8	−0.3	−27.1	−50.2	23.1	51.4
B3	−17.5	1.0	−16.5	1.9	−14.6	−44.8	30.2	47.7
TS(B1-C)	53.9	−0.2	53.7	−0.1	53.6	−50.3	103.9	50.0
TS(B2-C)	50.4	−0.4	50.0	−0.3	49.7	−51.2	100.9	50.5
TS(B3-C)	21.3	0.5	21.8	−0.3	21.5	−51.1	72.6	51.3
C	−64.4	6.0	−58.4	−1.4	−59.8	−52.6	−7.2	57.2
CC	121.5	7.7	129.2	5.9	135.1	−91.0	226.1	104.6
D1	−117.8	13.1	−104.7	−1.3	−106.0	−90.0	−16.0	101.8
D2	−126.4	13.2	−113.2	−3.1	−116.3	−94.4	−21.9	104.5
D3	−100.3	11.6	−88.7	−2.5	−91.2	−93.8	2.6	102.9
TS(D1-A1)	−49.9	12.4	−37.5	−3.1	−40.6	−94.0	53.4	103.3
TS(D3-A1)	−23.1	10.1	−13.0	−2.0	−15.0	−92.9	77.9	101.0
TS(D3-A2)	−43.8	11.3	−32.5	−2.2	−34.7	−87.9	53.2	97.0
A1[d]	−73.4	11.3	−62.1	−5.6	−67.7	−46.6	−21.1	52.3

[a] The correction term for zero-point energy. [b]The correction term for energy of thermal motion. [c]Energy is estimated with respect to **A1(NH4)** + CH_3I. [d]Energy of free CH_3COI added to complex **A1**.

higher in energy. The greater stability of species **D1** and **D2** relative to complex **D3** can be rationalized in terms of the trans influence; in the latter isomer two ligands possessing the ability to strongly destabilize trans Rh−ligand bonds, acyl and CO, are located in trans position to each other, thus destabilizing this isomer. Isomer **D2** is slightly preferred in energy over **D1** because of the more favorable orientation of the sterically asymmetric CH_3CO ligand (see Figure 2). Thus, with these calculations, we are able to confirm experimental results;[16] the trans complex **D2** has been deduced to be thermodynamically most stable based on the observation of one strong and one weak carbonyl signal in the IR spectrum. Nevertheless, a final conclusion about the preferred structure of **D** species has to await the discussion of activation barriers of **D**-type complexes.

3.2. Transition States. The catalytic cycle of methanol carbonylation (Figure 1) involves four elementary reaction steps, three of which are activated: CH_3I oxidative addition, CO migratory insertion, and CH_3COI reductive elimination. In the following, we will denote a transition state, **TS**, by both the corresponding

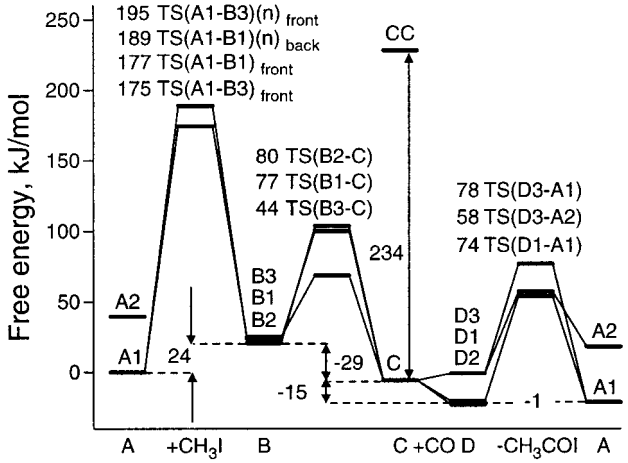

Figure 6. Free energy profile of the catalytic cycle of methanol carbonylation to acetic acid in the gas phase. Reaction energies are provided for the most favorable reaction path **A1** → **B1** → **C** → **D1** → **A1**. The energies of the transition states are given relative to corresponding reactants.

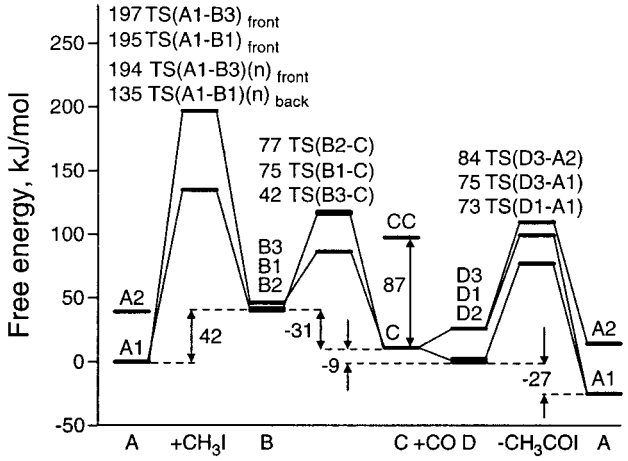

Figure 7. Free energy profile of the catalytic cycle of methanol carbonylation to acetic acid including solvent effects. Reaction energies are provided for the most favorable reaction path **A1** → **B1** → **C** → **D1** → **A1**. The energies of the transition states are given relative to corresponding reactants.

reactant and product configurations. Also, we will refer to the two types of transition states for the oxidative addition of CH_3I (specifying two different mechanisms of this reaction) as "front" and "back" (see Figures 4 and 5). We begin by examining each reaction individually. Subsequently, we will discuss the overall potential energy profile.

3.2.1. Oxidative Addition. The mechanism of the oxidative addition of a halogen−methyl substrate to a d^8 square-planar complex has been the subject of intensive debate.[39−41] In contrast to the addition of nonpolar molecules such as CH_4,[42,43] H_2,[8] and SiH_4[5] representing examples of nonionic single-step concerted addition, the insertion of a polar substrate such as a methyl halide was proposed to proceed according to the ionic two-step S_N2 mechanism as "back-side" attack of a methyl group by the Rh center. This leads to an inversion of the configuration at the methyl carbon center.[18,44] An alternative mechanism, the concerted cis addition of the halogen−alkyl bond to the metal center, proceeds with retention of the stereochemistry at the carbon atom. However, this mechanism has been rejected for polar molecules as unfavorable based on computational[45] and experimental results.[46] Transition states for CH_3I oxidative addition to *cis*-$[Rh(CO)_2I_2]^-$ complex corresponding to both types of mechanisms have already been located using a restricted Hartree−Fock approach,[18] and we intend to compare the reported results with those of our density functional calculations. Only CH_3I addition to complex **A1** will be discussed; we refrained from considering the reactions of the less stable complex **A2**.

The S_N2 oxidative addition of simple substrates such as CH_3I to square-planar complexes is assumed to proceed via a stepwise mechanism. The first step includes the substitution of iodide by the metal complex, i.e., addition of the ion metal complex to the carbon of CH_3I and the simultaneous expulsion of an iodide ion to form a five-coordinated neutral species $[Rh(CO)_2I_2CH_3]$. The subsequent addition of an iodide ligand to the free coordination site of the neutral complex completes the oxidative addition step to give a six-coordinated complex **B**. Since this mechanism involves the expulsion of an anion, I^-, the process is known to be difficult to describe by common density functional methods.[47] To reduce the effect of charge separation, NH_4^+ was introduced as a model counterion to accept the leaving iodide group; cations NBu_4^+ are used in the experiment.[12] To distinguish the transition states of these neutral NH_4^+-coordinated systems from those where the cation NH_4^+ is not explicitly taken into account, we use the extra designator (**n**).

The structure of the transition state of this back-side mechanism, **TS(A1-B1)(n)$_{back}$**, is presented in Figure 4; selected bond distances are given in Table 2. In **TS(A1-B1)(n)$_{back}$** the Rh center of the complex $[Rh(CO)_2I_2]^-$ is attacked by the carbon of methyl iodide with the iodide atom turned away from the plane of the complex. CH_3I approaches the plane of the metal complex at an angle I1−C1−Rh of 140°; the CH_3 moiety is almost planar. The Rh−methyl bond to be formed, Rh−C1 in **TS(A1-B1)(n)$_{back}$**, is about 0.8 Å longer than in product complex **B1**, while the breaking bond C1−I1 is stretched by only 0.4 Å compared to the reactant CH_3I. Thus, **TS(A1-B1)(n)$_{back}$** is an "early" transition state from the point of view of bond formation and breaking. This result differs from that obtained in previous HF calculations where the transition state termed "linear"[18] (which corresponds to the back-side mechanism of CH_3I addition to cis complex $[Rh(CO)_2I_2]^-$) was characterized as "very late". At the transition state, the Rh−C bond distance was calculated as 2.19 Å[18] (cf. 2.96 Å for Rh−C1 in present work), whereas the C−I bond length, 3.20

(39) Labinger, J. A.; Osborn, J. A. *Inorg. Chem.* **1980**, *19*, 3230.
(40) Labinger, J. A.; Osborn, J. A.; Coville, N. J. *Inorg. Chem.* **1980**, *19*, 3236.
(41) Pearson, R. G.; Muir, W. R. *J. Am. Chem. Soc.* **1970**, *92*, 5519.
(42) Margl, P.; Blöchl, P. E. *J. Am. Chem. Soc.* **1995**, *117*, 12625.
(43) Musaev, D. G.; Morokuma, K. *J. Organomet. Chem.* **1995**, *504*, 93.
(44) Fleming, I. *Frontier Orbitals and Organic Reactions*; Wiley: New York, 1976.
(45) Glukhovtsev, M. N.; Pross, A.; Schlegel, H. B.; Bach, R. D.; Radom, L., *J. Am. Chem. Soc.* **1996**, *118*, 11258.
(46) Su, T.; Morris, R. A.; Viggiano, A. A.; Paulson, J. F. *J. Phys. Chem.* **1990**, *94*, 8426.
(47) Rösch, N.; Trickey, S. B. *J. Chem. Phys.* **1997**, *106* (21), 8940.

Å[18] was found to be rather long (2.54 Å in the present work). However, since HF calculations lack correlation effects, they are known to be in general inadequate for describing transition metal−ligand bonds with strong d-character and intrabond correlation,[35,48] let alone the corresponding transition states. Therefore, the transition state structure located in the present work with a density functional method (that includes correlation effects) with partial inclusion of environment effects (via the model solvent ion NH_4^+) is considered to be more adequate.

Although the "front-side" mechanism of the CH_3I approach to the Rh center of $[Rh(CO)_2I_2]^-$ is expected to be kinetically less favored,[44] we located the alternative transition state **TS(A1-B3)(n)$_{front}$** (Figure 4). To allow a direct comparison with the "back-side" mechanism discussed above, we also took a coordinating NH_4^+ moiety into account during the optimization. Selected bond distances of the transition state **TS(A1-B3)(n)$_{front}$** are presented in Table 2. The transition state has a trigonal bipyramidal structure and can be considered as a η^2-adduct of a butterfly-shaped fragment $[Rh(CO)_2I_2]^-$ and a methyliodide with an elongated C−I bond (see Figure 4). The newly formed bond Rh−I1 of the transition state is only 0.15 Å longer than that of the product complex **B3**. On the other hand, the second newly formed bond—Rh−C1(methyl) of **TS(A1-B3)(n)$_{front}$**—is 0.7 Å longer than the corresponding bond distance, Rh−C2, of the complex **B** (cf. Tables 1 and 2). Thus, the side-on approach of CH_3I does not seem to be a concerted process; rather the rhodium−iodine bond is formed first, followed by the formation of the rhodium−methyl bond. The methyl−iodide bond C1−I1 in the transition state is significantly longer than in a free CH_3I molecule and in **TS(A1-B1)(n)$_{back}$**. In **TS(A1-B3)(n)$_{front}$**, the C1−I1 bond distance was calculated as 2.71 Å compared to 2.19 Å in CH_3I and 2.54 in **TS(A1-B1)(n)$_{back}$**. Thus, the transition state **TS(A1-B3)(n)$_{front}$**, which corresponds to a front-side approach of CH_3I, can be characterized as "late", at variance with the nature of **TS(A1-B1)(n)$_{back}$**.

To estimate the effect of the NH_4^+ group on the structure and activation barrier, we also located transition states that correspond to the "front-side" approach of CH_3I in side-on fashion to the Rh center of complex **A1** in the absence of a counterion NH_4^+ (Figure 5). Pertinent bond distances of the transition states **TS(A1-B1)$_{front}$** and **TS(A1-B3)$_{front}$** are presented in Table 2. Their structures are quite similar to those of **TS(A1-B3)(n)$_{front}$**, but some differences are worth mentioning. The newly formed bonds Rh−I1 and Rh−C1 are 0.02−0.03 and 0.1 Å shorter than those of the NH_4^+-coordinated transition state **TS(A1-B3)(n)$_{front}$**. Similarly, the bond to be broken, C1−I1, is shortened by 0.03−0.08 Å compared to that of the corresponding neutral system. Thus, consideration of the counterion induces some geometry changes, but it does not change the character of the transition state from the point of view of bond formation and breaking.

Addition of the counterion NH_4^+ weakly affects the activation barriers. The NH_4^+-coordinated transition state **TS(A1-B3)(n)$_{front}$** has an activation energy of 158 kJ/mol (Table 5). Its charged analogues **TS(A1-B1)$_{front}$** and **TS(A1-B3)$_{front}$** are 136 and 132 kJ/mol less stable than the corresponding reactants. The energies of **TS(A1-B1)$_{front}$** and **TS(A1-B3)$_{front}$** were estimated relative to those of the separate reactants **A1** and CH_3I, whereas the energies of the NH_4^+-coordinated transition states **TS(A1-B1)(n)$_{back}$** and **TS(A1-B3)(n)$_{front}$** were calculated relative to that of species **A1(NH$_4$)** (i.e., complex **A1** "solvated" by a NH_4^+ ion; Figure 4) and free CH_3I. The barrier of the transition state for the back-side attack of CH_3I, **TS(A1-B1)(n)$_{back}$**, was estimated to 146 kJ/mol, which is 12 kJ/mol lower than that of the corresponding front-side attack, **TS(A1-B3)(n)$_{front}$**. Thus, for the gas phase we confirm the preference of the back-side mechanism of CH_3I oxidative addition as previously reported.[18] However, our results differ from those earlier ones[18] (calculated at the MP2 level in single-point fashion) with regard to the activation barriers of the transition states of both mechanisms. With wave function based methods,[18] the activation energy of the linear TS, which corresponds to a back-side approach of CH_3I, was calculated as 71 kJ/mol, i.e., 75 kJ/mol lower than the present DF result for the barrier **TS(A1-B1)(n)$_{back}$**. The MP2//HF activation energy of the bent TS (255 kJ/mol),[18] which results from front-side attack of CH_3I, is overestimated by 97 kJ/mol compared to our DF result. Note, however, these latter data are based on HF geometries which are quite different from those of the present work, optimized at the DF level (see above).

On the basis of the activation barriers calculated for the two different mechanisms of methyliodide addition to the square-planar complex **A1**, via the back-side and the front-side approach, we conclude that in the gas phase the back-side attack of **A1** is preferred. The oxidative addition reaction is exothermic in the gas phase; both products **B1** and **B3** are 23−25 kJ/mol more stable than the separate reactants, CH_3I and complex **A1** (Table 4).

Inclusion of solvent effects on reactants, transition states, and products is required to achieve realistic estimates of the energetics of various elementary steps of the catalytic cycle. In particular, activation barriers have to be corrected for solvent effects of the medium surrounding the active complex. We postpone the discussion of solvent effects on activation barriers and reaction energies to section 3.3.

3.2.2. Migratory CO Insertion. Migratory CO insertion takes place in the six-coordinated complex **B** to produce the five-coordinated complex **C**. Since three isomers are possible for complex **B**, three reaction paths connecting the corresponding species **B** to complex **C** have been investigated. The corresponding transition states **TS(B1-C)**, **TS(B2-C)**, and **TS(B3-C)** are shown in Figure 5; for pertinent bond distances, see Table 2.

All these transition states involve rearrangements of three centers, and they all have a trigonal bipyramidal structure with a partially formed CH_3CO fragment as one of the ligands in the equatorial plane (Figure 5). **TS(B3-C)** exhibits the shortest Rh−CH_3 bond distance (Rh−C1), 2.319 Å, compared to 2.369 and 2.378 Å of **TS(B1-C)** and **TS(B2-C)**. It also features the longest distance of the C−C bond to be formed (C1−C2, Table 2), 1.968 Å, compared to 1.937 and 1.853 Å of **TS(B1-**

(48) Görling, A.; Trickey, S. B.; Gisdakis, P.; Rösch, N. In *Topics in Organometallic Chemistry*; Brown, J., Hofmann, P., Eds.; Springer: Heidelberg, 1999; Vol. 4, p 109.

C) and **TS(B2-C)**, respectively. In **TS(B3-C)**, the Rh−methyl bond is stretched by 0.19 Å only compared to the reactant **B3**, while the newly formed C−C bond is 0.44 Å longer than in the product **C**. This suggests that the transition state **TS(B3-C)** occurs early along the reaction path. The other two transition states, **TS(B1-C)** and **TS(B2-C)**, are somewhat product-like, i.e., later along the reaction coordinate. The Rh−CH_3 distances are 0.22−0.23 Å longer than in reactants **B1** and **B2** and the C1−C2 distances are 0.32−0.41 Å longer than in product **C**, but still closer to the distance of the reactants **B1** and **B2** than to that of the product **C**.

The transition states **TS(B1-C)** and **TS(B2-C)** have larger activation energies (76 and 81 kJ/mol, respectively) than **TS(B3-C)**, which features the smallest barrier, 40 kJ/mol (Table 2). This result may be rationalized by the observation that in **TS(B3-C)** a strong trans effect of CO facilitates the stretching and breaking of the Rh−CH_3 bond in the trans position, thus reducing the activation barrier of this TS. In the other two transition states, **TS(B1-C)** and **TS(B2-C)**, an iodide is in trans position to the CH_3 group, which decreases the activation barrier less, due to a weaker trans influence. The dependence of the activation barrier height upon the ability of the ligand trans to the migrating CH_3 group to destabilize the metal−methyl bond has already been pointed out in a recent DF study.[19] There, activation barriers for transition states with I (78 kJ/mol) and CO (53 kJ/mol) trans to the methyl group have been reported;[19] these values agree quite well with the present results for the analogous transition states **TS(B1-C)** and **TS(B3-C)**, in particular since somewhat different computational methodologies have been employed in the two cases.

The CO insertion step is exothermic (Table 4); the calculated reaction energies of the various elementary reactions are very similar: −37, −32, and −40 kJ/mol for the paths **B1** → **C**, **B2** → **C**, and **B3** → **C**. The energetics of the migratory insertion of CO into the Mn−methyl bond of $CH_3Mn(CO)_5$,[49] calculated with the Hartree−Fock−Slater (local density functional) method, are similar to our results. This reaction[49] was calculated to proceed with an activation barrier of 75 kJ/mol and a reaction energy of −75 kJ/mol. These present energy data are quite different from those of the BP calculation for CO insertion in $RhH(CO)(PH_3)_2Cl$ complexes.[10] There, higher activation barriers, 114 and 129 kJ/mol, were calculated for cis and trans isomers of the rhodium complex, and the reaction was found to be exothermic by only 13 kJ/mol. The lower value of the activation barrier for the step **B** → **C** can be rationalized by the stabilization of the TS due to the presence of the two carbonyl groups, which are known to be good π-accepting ligands.

3.2.3. Reductive Elimination. By uptake of a CO ligand into the free octahedral coordination site, complex **C** transforms into **D** species, the precursor complex for reductive elimination. During this step, a comparatively strong bond is formed and no bonds are broken; therefore, we refrained from studying transition structures. In fact, the reaction is quite exothermic with reaction energies of −59, −65, and −39 kJ/mol for the reactions **C** → **D1**, **C** → **D2**, and **C** → **D3**, respectively (Table 4).

The last elementary step of the catalytic cycle (Figure 1) is the reductive elimination of acetyliodide from the octahedral complex **D**. The reductive elimination of CH_3COI from species **D1** and **D2** with carbonyl groups cis and trans to each other, respectively, leads to the corresponding four-coordinated cis and trans complexes **A1** and **A2**. Elimination of CH_3COI from complex **D3** produces either the cis complex **A1** or the trans complex **A2**. Thus, there are four possible routes for the transformation of **D**-type species into isomers of complex **A**. The structures of three of these transition states are presented in Figure 5; see Table 2 for pertinent bond distances.

Transition states **TS(D1-A1)** and **TS(D3-A1)** have trigonal bipyramidal structures (Figure 5) and can be viewed as η^2-adducts of the butterfly-shaped fragment $Rh(CO)_2I_2$ and an elongated carbon−iodine σ-bond of the CH_3COI fragment, similar to the transition states for CH_3I oxidative addition (section 3.2.1.). Note that in **TS(D1-A1)** the breaking bonds Rh−I2 and Rh−C_{acyl} are 0.55 and 0.45 Å, respectively, longer than the corresponding bonds Rh−I1 and Rh−C2 of the reactant **D1**. Because of this rather uniform bond elongation, acetyliodide elimination via **TS(D1-A1)** can be considered concerted (with respect to the cleavage of the Rh−I2 and Rh−C_{acyl} bonds). In contrast, in **TS(D3-A1)** the bonds to be broken, Rh−I2 and Rh−C2, are 0.21 and 0.76 Å, respectively, longer than the bonds Rh−I1 and Rh−C2 of the reactant complex **B3**. Hence, acetyliodide elimination via **TS(D3-A1)** does not follow a concerted mechanism; rather, the Rh−C_{acyl} bond is broken first. The newly formed C−I bond (C2−I2, Table 2) is only 0.22 and 0.19 Å longer than that of free acetyliodide, 2.30 Å (Table 2), indicating that both transition states are product-like ("late"). On the other hand, **TS(D3-A2)** features an almost planar fragment $Rh(CO)_2I_2$, which interacts with acetyliodide only by coordination of the carbonyl carbon to the rhodium center; the distance Rh−C2 is 2.783 Å. Iodine is transferred to the acetyl fragment; the distance Rh−I2 is 3.97 Å, compared to 2.86 Å in the initial complex **D3**. The newly formed C−I bond of acetyliodide is shorter than in the other two transition states and only 0.15 Å longer than in free CH_3COI. The rather long bond distances Rh−C_{acyl} and Rh−I and the shorter C−I distance show that **TS(D3-A2)** is closest in structure to the products; the interaction between the moieties CH_3COI and $Rh(CO)_2I_2$ of this transition state is weaker than in the transition states leading to complex **A1**. The search for the transition state along the path from the reactant **D2** to the product **A2** was found to converge to the transition state structure **TS(D3-A2)**.

The activation energies of the three transition states **TS(D3-A1)**, **TS(D1-A1)**, and **TS(D3-A2)** for reductive elimination are 80, 73, and 64 kJ/mol, respectively (Table 2). Reductive elimination of acetyliodide was found to be endothermic with reaction energies of 49, 29, 66, and 92 kJ/mol for the paths **D1** → **A1**, **D3** → **A1**, **D3** → **A2**, and **D2** → **A2**, respectively (Table 4).

The transition states located for the reductive elimination of CH_3COI can also be considered as transition structures of the reverse process, namely, CH_3COI

(49) Ziegler, T.; Versluis, L.; Tschinke, V. *J. Am Chem. Soc.* **1986**, *108*, 612.

oxidative addition to the square-planar complex $[Rh(CO)_2I_2]^-$. From this point of view, it is interesting to compare the reaction energies and energies of activation for the oxidative addition of acetyliodide and methyliodide to rhodium complexes of type **A**. The reaction with acetyliodide proceeds via a front-side attack of the C−I bond of CH_3COI by the species **A** (Figure 5). Addition of the C−I bond in η^2 fashion in the steps **A1** → **D1**, **A2** → **D3**, and **A1** → **D3** exhibits activation energies of 24, −2, and 51 kJ/mol, respectively. The located transition states are reactant-like with respect to CH_3COI oxidative addition process. The analogous side-on approach of CH_3I to complex **A** proceeds with a much higher activation energy of 132 and 136 kJ/mol. In contrast to the acetyliodide oxidative addition process, transition states of CH_3I addition are product-like. The addition of CH_3COI to the rhodium complex **A** is more exothermic (−49, −29, −92, and −66 kJ/mol for the reactions **A1** → **D1**, **A1** → **D3**, **A2** → **D2**, and **A2** → **D3**, respectively) than the addition of CH_3I (−25, −23, −68, and −60 kJ/mol for the reactions **A1** → **B1**, **A1** → **B3**, **A2** → **B2**, and **A2** → **B3**; Table 4).

3.3. Solvent Effects. All calculations discussed so far represent situations in the gas phase. Actually, methanol carbonylation proceeds in solution, and in particular due to the presence of ions, environment effects play an important role in determining the corresponding potential energy surface.

In our estimates of these environment effects, dichloromethane was chosen as medium since this solvent is used in experiment.[12] These estimates (Table 4) were obtained in single-point calculations for optimized structures at the stationary points.

One notes that the dimer **CC** of the complex **C** has the largest solvation energy (−409 kJ/mol; see Table 4) because this complex carries the largest negative charge, −2 e, of the systems under study. Among the species with charge −1 e, the unsaturated four-coordinated complex **A** exhibits the most significant solvent effects, −138 kJ/mol for **A1** and **A2** (Table 4). The five-coordinated complex **C** undergoes a somewhat smaller stabilization due to the solvent (ΔG_{solv} = −130 kJ/mol) than complexes **A**. The saturated six-coordinated complexes **B** (ΔG_{solv} = −126−129 kJ/mol) and **D** (ΔG_{solv} = −122−125 kJ/mol) have the smallest solvation energies (by absolute value) among the complexes of charge −1 e. Thus, one notes that the solvent stabilization energy increases (in absolute value) along the series **D** < **B** < **C** < **A**, i.e., for complexes with 6-fold < 5-fold < 4-fold coordination.

The solvent effect of the neutral complex **A1(NH$_4$)**, i.e., complex **A1** coordinated with NH_4^+ (Figure 4), features a much smaller solvent stabilization (−31 kJ/mol; Table 4) than the charged intermediates discussed previously.

In Table 4, we present also the solvent effects on the transition structures. Transition states **TS(A1-B1)$_{front}$** and **TS(A1-B3)$_{front}$**, leading from **A** to **B** via the side-on mechanism, feature solvation energies very similar to those of the product complexes **B1** and **B3**, −129 and −125 kJ/mol, respectively. This finding is easily rationalized by the fact that these transition states can be characterized as rather product-like. Analogous statements hold for the early **TS(B3-C)** of CO migratory insertion with solvent effects similar to those of the corresponding reactant. Also, the transition states **TS(B1-C)** and **TS(B2-C)** of CO migratory insertion are late transition states, with solvation energies similar to those of the corresponding products.

It is of crucial importance that the solvent effect on **TS(A1-B1)(n)$_{back}$**, i.e., the neutral NH_4^+-coordinated transition state leading from **A** to **B** via the back-side mechanism, −94 kJ/mol, is 3 times larger than the solvent stabilization of the reactant complex **A1(NH$_4$)**. Thus, solvent effects stabilize **TS(A1-B1)(n)$_{back}$** with respect to the reactants, while they destabilize the alternative structures **TS(A1-B1)$_{front}$** and **TS(A1-B3)$_{front}$** compared to the reactant complex **A1**. The solvent effect of the NH_4^+-coordinated transition state for the front-side approach **TS(A1-B3)(n)$_{front}$**, 42 kJ/mol, is close to that of the neutral complex **A1(NH$_4$)** and thus does not entail a reduction of the activation barrier. As just noted, the solvation energies of **TS(B1-C)** and **TS(B2-C)**, −131 kJ/mol for both structures, are similar to that of complex **C**, while **TS(B3-C)** features a solvent effect (−128 kJ/mol) closer to the reactant **B3**. Two of the transition states of the step **D** → **A**, **TS(D1-A1)** and **TS(D3-A1)**, show solvation energies, −124 and −127 kJ/mol, similar to the six-coordinated complexes **D**. It is important to notice that **TS(D3-A2)** is stabilized in solution by −96 kJ/mol only. Thus, with the exception of NH_4^+-coordinated transition states, **TS(A1-B1)(n)$_{back}$** and **TS(A1-B3)(n)$_{front}$**, and of **TS(D3-A2)**, one can conclude that the solvent stabilization of all other transition states is similar to that of the saturated six-coordinated complexes **B** and **D**.

3.4. Potential Energy Profile of the Full Catalytic Cycle. Finally, we will combine the relative energies of intermediates and transition states of the various elementary steps discussed above to construct the energy profile of the entire catalytic cycle; we will also take solvent effects into account. Since most of the intermediates have isomers, there are various alternative reaction pathways that connect reactants and products. By comparing the calculated activation energies of the elementary reactions we are able to extract the most favorable path of the catalytic process.

Let us first discuss the potential energy profile based on gas phase relative energies ΔE(X→Y); see Table 4. The catalytic cycle starts from complex **A1**, which is more stable than isomer **A2**. **A1** transforms into **B1** via transition state **TS(A1-B1)(n)$_{back}$**, which corresponds to a back-side mechanism with an activation energy that is 12 kJ/mol lower than that of the alternative transition state **TS(A1-B3)(n)$_{front}$** of the front-side mechanism. In the migatory insertion step the activation barrier from **B3** to **C** was calculated to be the smallest among the possible paths. CO coordination to **C** leads to **D2**, the most stable isomer among the **D**-type complexes. In the reductive elimination step the path of lowest energy starts from **D1** and results in **A1** via transition state **TS(D1-A1)**. Thus, the most favorable reaction pathway in the gas phase is **A1** → **B1** → **B3** → **C** → **D2** → **D1** → **A1**.

The catalytic cycle includes reactions that proceed with a change of the number of independent particles; that is, it includes association (CH_3I oxidative addition and CO uptake) and dissociation steps (CH_3COI reduc-

tive elimination). The entropy contributions of such processes are known to be significant. Different contributions to the free energy are given in Table 5. The free energy profile of the gas phase process is presented in Figure 6. The CH_3I oxidative addition step remains rate-limiting; that is, it features the highest activation barrier. As expected for an association reaction, the entropy contribution increases this barrier further, by 43 kJ/mol (Table 5). Similar effects are responsible for the destabilization of the oxidative addition product **B** with respect to reactants, e.g., ΔE(**A1**→**B1**) = −25 kJ/mol, ΔG(**A1**→**B1**) = 24 kJ/mol.

Among the most significant differences between the energy and free energy profiles are the reaction energies for the steps **C** → **D** (e.g., ΔE(**C**→**D1**) = −59 kJ/mol, ΔG(**C**→**D1**) = −15 kJ/mol) and **D**→**A** (e.g., ΔE(**D1**→**A1**) = 49 kJ/mol, ΔG(**D1**→**A1**) = −1 kJ/mol) as well as the energy of the overall catalytic cycle (ΔE(**A1** + CH_3I + CO → **A1** + CH_3COI) = −73 kJ/mol; ΔG(**A1** + CH_3I + CO → **A1** + CH_3COI) = −23 kJ/mol). Entropy effects on CO migration and CH_3COI reductive elimination barriers are modest and do not exceed 6 kJ/mol since the underlying transformations **B** → **TS(B-C)** and **D** → **TS(D-A)** do not entail changes in the number of independent species. Thus, while inclusion of entropy corrections does not change the most favorable reaction path, it renders the potential energy profile smoother (cf. Figures 6 and 7).

Finally, let us discuss the free energy profile with solvent effects included. The catalytic cycle starts with complex **A1**, which is 39 kJ/mol more stable than isomer **A2** in the gas phase as well as in solution (Table 4). Addition of CH_3I to **A1** yields either **B1** or **B3** and in solution proceeds with reaction energies of 42 and 47 kJ/mol, respectively (compared to 24 and 25 kJ/mol in the gas phase; see Table 4 as well as Figures 6 and 7). The activation barrier of the step **A** → **B** via a back-side attack of CH_3I is lowered by solvent effects, to ΔG_{final}(**A1(NH$_4$)**→**TS(A1-B1)(n)$_{back}$**) = 135 kJ/mol (Table 4); this barrier is smaller than that of alternative mechanisms, e.g., a front-side attack of CH_3I with a barrier (corrected for solvent effects) of ΔG_{final}(**A1**→**TS(A1-B3)(n)$_{front}$**) = 194 kJ/mol (Table 4). It is very important to notice that solvent effects stabilize the back-side transition state **TS(A1-B1)(n)$_{back}$** by 54 kJ/mol, whereas the barrier of the front-side transition state **TS(A1-B3)(n)$_{front}$** is not changed in solution. Thus, the preference of back-side mechanism of CH_3I addition over side-on addition is much stronger in the condensed phase (59 kJ/mol) than in the gas phase (6 kJ/mol). The activation barrier of the next step, CO migration, is lower for the process **B3** → **C** (44 kJ/mol in the gas phase; 42 kJ/mol in solution) than the barriers of the alternative pathways **B2** → **C** (80 and 77 kJ/mol in the gas phase and solution, respectively) and **B1** → **C** (77 and 75 kJ/mol without and with inclusion of solvent effects, respectively). In solution, all **B**-type intermediates are essentially degenerate, within 6 kJ/mol. CO coordination to species **C** leads to the most stable isomer **D2** of complex **D**. After isomerization to complex **D1** (with a reaction energy of 2 kJ/mol in solution), this latter complex decomposes, yielding acetyliodide and the initial complex **A1** with the lowest activation barrier, 75 kJ/mol in dichloromethane (see Figure 7). With a barrier of ΔG(**D3**→**A2**) = 58 kJ/mol, the reaction path from **D3** to complex **A2** is most favorable in the gas phase, whereas in solution this path has the highest activation barrier (84 kJ/mol). Thus, in solution the most likely reaction path of the full catalytic cycle is **A1** → **B1** → **B3** → **C** → **D2** → **D1** → **A1**. The energy difference between the end point of the full catalytic cycle, **A1** + CH_3COI, and the starting point of the cycle, **A1** + CH_3I + CO, is the reaction energy of CO insertion into the carbon−iodine bond of CH_3I, −25 kJ/mol; that is, the overall reaction is exothermic.

Thus, according to our density functional calculations, the CH_3I oxidative addition reaction is the rate-determining step of the methanol carbonylation process. That first activation barrier was calculated as 135 kJ/mol, compared to 100 kJ/mol in experiment.[20] The activation barrier for the CO insertion step is much smaller than that of the first step. For the transformation via **TS(B3-C)**, starting from the cis complex **B3** with inequivalent carbonyl groups, it is estimated to be 44 kJ/mol. The barriers for **TS(B1-C)** and **TS(B2-C)** (starting from the cis and trans complexes **B1** and **B2**, respectively, with equivalent CO groups) are 75 and 77 kJ/mol. Since complex **B** was found to preferentially exist as isomers **B1** or **B2**, it is more reasonable to compare the experimental barrier for CO migration with those of **TS(B1-C)** or **TS(B2-C)** (rather than with that of **TS(B3-C)**). Both these values are in excellent agreement with the experimental value of 81 kJ/mol.[20] The activation energy of the final step of the catalytic cycle, CH_3COI reductive elimination, 75 kJ/mol, is somewhat lower than the approximate experimental value, 100 kJ/mol.[20] This final barrier is comparable with that of the CO insertion reaction, but lower than that of the initial oxidative addition step.

In summary, inclusion of solvent effects has crucial consequences for the shape of the reaction profile. In particular, solvation of the coordinately unsaturated four-coordinated complex **A** makes the product of the oxidative addition reaction, complex **B**, thermodynamically less stable with respect to the reactants. Thus, it becomes clear that the oxidative addition step is rate-determining due to unfavorable kinetics (high activation energy) as well as thermodynamics (endothermic heat of reaction). On the other hand, the stabilization of species **A** in solution renders the final reductive elimination step more exothermic, thus facilitating that step (ΔG(**D1-A1**) = −1 kJ/mol, ΔG_{final}(**D1-A1**) = −27 kJ/mol). The stronger solvation of the five-coordinated species **C** compared to the 6-fold coordinated complexes **D** leads to a destabilization of the latter by 6−8 kJ/mol in dichloromethane. The formation of the dimer **CC** resulting from the dimerization of complex **C** was calculated to be much more favorable in solution (87 kJ/mol) than in the gas phase (234 kJ/mol), but it is endothermic in either case. The preference of back-side mechanism for the oxidative addition of CH_3I to the square-planar complex **A** via **TS(A1-B1)(n)$_{back}$** over the corresponding front-side process certainly remains the most dramatic solvent effect during the whole catalytic cycle.

4. Conclusions

We have carried out a density functional study of the full methanol carbonylation cycle catalyzed by the

rhodium complex $[Rh(CO)_2I_2]^-$. We have investigated the molecular structures of various catalytically active intermediates involved in methanol carbonylation cycle as developed by Forster[2] (Figure 1): the complexes **A** $[Rh(CO)_2I_2]^-$, **B** $[RhCH_3(CO)_2I_3]^-$, **C** $[Rh(CH_3CO)(CO)I_3]^-$, and **D** $[Rh(CH_3CO)(CO)_2I_3]^-$.

The preference for the cis conformation of complex **A** and the trans conformation of complex **D** found in the present work is in agreement with available experimental data. In contrast to the interpretation of experimental data,[12] the calculations showed complex **B** to be most stable in the trans conformation.

We were able to locate the transition states of three elementary reaction steps. These computational results corroborate[20] that the rate-determining step of the methanol carbonylation is the CH_3I oxidative addition reaction with a calculated activation barrier of 135 kJ/mol. The calculations also confirmed that the decomposition of the kinetically unstable complex **B** is due to fast migratory insertion **B** → **C** reaction (ΔG_{final} = 75 kJ/mol) rather than due to reductive elimination **B** → **A** (ΔG_{final} = 93 kJ/mol, Figure 7). The activation barrier of the final CH_3COI reductive elimination step **D** → **A** was calculated to be 60 kJ/mol lower than that of the CH_3I oxidative addition step **A** → **B**.

Solvent effects were found to be of crucial importance for estimating the barrier of the rate-determining step **A** → **B** and, thus, for delineating the overall reaction profile.

On the basis of the calculated reaction energies and activation barriers of the elementary steps of the catalytic cycle, we proposed the reaction path **A1** → **B1** → **B3** → **C** → **D2** → **D1** → **A1** as most favorable for methanol carbonylation (see Figure 7).

Acknowledgment. We thank G. N. Vayssilov for helpful suggestions. This work was supported by Volkswagen Foundation (grant no. I/73 653), INTAS-RFBR (grant no. IR-97-1071, RFBR no. 97-03-71057), Krasnoyarsk Regional Scientific Foundation (grants no. 1F0161, 6F0151), and Fonds der Chemischen Industrie.

Supporting Information Available: The geometries in Cartesian coordinates and absolute energies for all of the optimized intermediates and transition states. This material is available free of charge via the Internet at http://pubs.acs.org.

OM000761A